

Spatial elucidation of motion in proteins by ensemble-based structure calculation using exact NOEs

Beat Vögeli¹, Sina Kazemi², Peter Güntert^{2,3} & Roland Riek¹

Proteins are inherently dynamic systems whose motions cover large ranges in both magnitude and timescale. Because of the omnipresence of motion, it is likely that dynamics have important roles in the function of biomolecules. For detailed understanding of a protein's function, the three-dimensional structure and description of its dynamics are therefore required. Structure determination methods are well established, and NMR-relaxation phenomena provide insights into local molecular dynamics; moreover, recently several attempts have been made to detect concerted motion. Here, we present an ensemble-based structure-determination protocol using ensemble-averaged distance restraints obtained from exact NOE rates. Application to the model protein GB3 establishes an ensemble of structures that reveals correlated motion across the β -sheet, concerted motion between the backbone and side chains localized in the structure core, and a lack of concerted conformational exchange between the β -sheet and the α -helix.

At physiologically relevant temperatures, proteins interchange between structural states covering a large range in magnitude from 10^{-11} to 10^{-6} m as well as spanning timescales from 10^{-12} s to 10^5 s and beyond. It is likely that evolution has taken advantage of this inherently dynamic nature of proteins, and thus dynamics may have important roles in the activity of proteins. To obtain a detailed description and understanding of a protein's function, its three-dimensional (3D) atomic-resolution structure and an accurate description of its entire dynamics are therefore required. NMR-relaxation phenomena provide a great deal of insight into local molecular dynamics. However, the dynamic picture is still largely incomplete because no adequate method is available to detect either motion through space or concerted motion. Attempts toward a comprehensive description of motion are currently under way through methods that include residual dipolar couplings (RDC), relaxation dispersion NMR, paramagnetic relaxation enhancement (PRE), cross-correlated relaxation (CCR) and conventional nuclear Overhauser enhancement (NOE) experiments in combination with molecular-dynamics simulations or structure-prediction software^{1–14}.

Whereas the description of the motion of a protein is still in its infancy, the structure determination of biomolecules by either X-ray

crystallography or NMR is well established. NMR structure determination of biomolecules is mainly based on a large collection of NOEs (Fig. 1a)¹⁵. For the structure calculation, the obtained semiquantitative NOEs are translated semiquantitatively into upper limit distances, following the proportionality of the NOE cross-relaxation rate with the inverse 6th power of the distance between two (isolated) interacting spins¹⁵. Such an approach usually results in a well-defined 3D NMR structure, as exemplified here for the 56-residue model protein GB3 (Fig. 1a). The input of 1,956 NOE-based upper-limit distance restraints, combined with 147 dihedral-angle restraints derived from scalar couplings, 54 dihedral-angle restraints from ¹³C α chemical shifts and 90 RDCs, yielded the 3D NMR structure of GB3, represented by a bundle of nine conformers reflecting the precision of the structure (Fig. 1a; backbone r.m.s. deviation of 0.47 Å). This practice dates back to the 1980s, when it proved difficult to determine NOE rates and convert them into exact distances¹⁵. In the following, we present an ensemble-based structure-determination protocol using ensemble-averaged distance restraints obtained from exact NOE rates recently introduced^{16–20}. When this approach is applied to the model protein GB3, a structural ensemble is obtained that describes its conformational space occupied, thereby reflecting both its 3D structure and its dynamics.

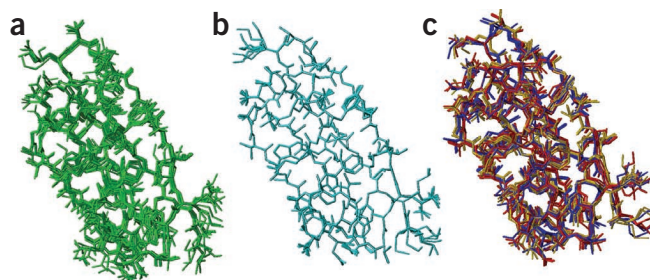
RESULTS

We recently demonstrated the collection of exact ¹H^N-¹H^N NOE rates (eNOE) by using state-of-the-art NMR spectrometers, optimized 3D-resolved [¹H,¹H]-NOESY experiments, short NOESY mixing times, an optimized protocol for extracting NOE rates from a series of NOESY spectra and spin-diffusion correction^{16,17}. Here, we extended the eNOE to aliphatic protons, establishing a data set of 823 eNOEs for the model protein GB3 (Table 1 and unpublished data). The eNOEs were converted into distances, based on the assumption that the NOE is mostly sensitive to slow motion. This was shown to be valid for H-H spin pairs if the local H-X order parameters, which are a measure of fast motion, are larger than 0.5 (refs. 20,21). This is most often the case in folded proteins. Even for lower-order parameters down to 0.2, the fast motion alters the eNOE-derived distances by less than 10% (ref. 21). Overall, the translation from eNOEs to distances is very robust because the $1/r^6$ dependency between NOE and distance

¹Laboratory of Physical Chemistry, Swiss Federal Institute of Technology, Zürich, Switzerland. ²Institute of Biophysical Chemistry, Center for Biomolecular Magnetic Resonance and Frankfurt Institute for Advanced Studies, J.W. Goethe-Universität, Frankfurt am Main, Germany. ³Graduate School of Science, Tokyo Metropolitan University, Tokyo, Japan. Correspondence should be addressed to R.R. (roland.riek@phys.chem.ethz.ch).

Received 6 December 2011; accepted 6 July 2012; published online 2 September 2012; doi:10.1038/nsmb.2355

Figure 1 Heavy-atom structural representations of GB3 following either the classical protocol with NOEs as experimental input, the classical protocol with eNOEs or the ensemble-based protocol with eNOEs. (a) Bundle calculated with a classical protocol based on standard NOE measurements. Nine conformers are shown. (b) Single-state bundle calculated with eNOEs. Nine conformers are shown. (c) Three three-state ensembles obtained from eNOEs. The three most similar structures from each three-state conformer are grouped in gold, red and blue.



reduces the relative distance error correspondingly compared to the relative inaccuracies of the NOE measurements^{16,17,21}. The eNOEs of GB3 yielded three classes of distance restraints (**Table 1**): (i) exact distances with an estimated accuracy of 5%, obtained from the eNOEs determined for two symmetric pathways (that is, from spin I_1 to I_2 and vice versa from I_2 to I_1), (ii) distances with an estimated accuracy of 15%, derived from single eNOEs pathways, and (iii) distances with an estimated accuracy of 20%, derived from methyl-methyl eNOEs for which additional corrections had to be added to the distance restraint, following established arguments^{15,22}.

The eNOE-derived distance restraints in combination with the small set of RDCs and angle restraints derived from scalar couplings and $^{13}\text{C}^\alpha$ chemical shifts were used for a structure calculation of GB3, following standard protocols using the software package CYANA^{23,24}. The bundle of nine conformers shown in **Figure 1b** represents the calculated structure. The input data resulted in an extremely tight, albeit not correct (see below), structure with a small backbone r.m.s. deviation of 0.11 Å and an all-heavy atom r.m.s. deviation of only 0.60 Å. When compared to the traditional structure calculation using semiquantitative NOEs, the high precision is particularly striking (compare **Figs. 1a** and **1b**). Furthermore, the eNOE-based single-state NMR structure coincides closely with the RDC-optimized X-ray structure of GB3 (refs. 25,26) with an r.m.s. deviation of 0.57 Å for the backbone and 1.17 Å for all heavy atoms (**Supplementary Fig. 1**). However, the large target-function value of 27.5 Å² (**Table 1** and **Fig. 2**), resulting from many distance-restraint violations, indicates that the structure does not agree with the experimental data. The large number of violations of experimental restraints can be attributed to the motion-averaged nature of the measured NOE, whereas the structure-calculation protocol is based on a single static structure, which obviously does not take into account any motion²⁷.

Following the ergodic hypothesis, the influence of motion of a protein on the NOE probe can be described by an ensemble of structural states. To include the motional dependence of the eNOEs in the structure calculation, an ensemble-based protocol was established within the software package CYANA. The protocol requests that the experimental restraints be fulfilled by a set of structural states rather

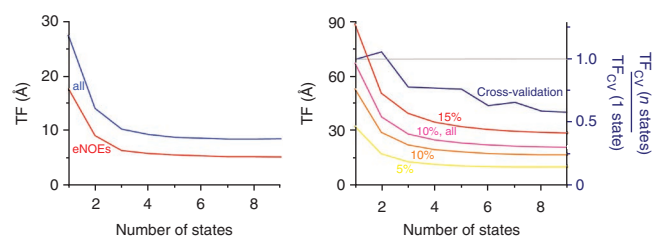
than by a single structure^{1–3}. To avoid divergence among the structural states that is not implied by the experimental restraints, we imposed ‘bundling restraints,’ weak harmonic restraints that minimize the distances between corresponding atoms in different states¹. Following this protocol, we obtained structures of GB3 represented by ensembles ranging from two to nine states. **Figure 2** illustrates the decrease in the target function when the increase in the number of states is

Table 1 NMR and refinement statistics for protein structures

	Three-state ensemble protocol using eNOEs	Single-state ensemble protocol using eNOEs	Standard protocol using NOEs
NMR distance and dihedral constraints			
Distance constraints			
Total NOE	884	884	1,041
eNOE	823	823	
eNOE from two pathways	324	324	
eNOE from one pathway	481	481	
eNOE between two methyl groups	18	18	
Standard NOE involving aromatics (upper limit 8 Å)	61	61	
Intra-residue	277	277	160
Inter-residue	607	607	881
Sequential ($ i - j = 1$)	244	244	299
Medium-range ($1 < i - j < 4$)	122	122	204
Long-range ($ i - j \geq 5$)	241	241	378
Total residual dipolar coupling restraints	90	90	90
^{15}N - ^1H N	47	47	47
^{13}C - ^1H α	43	43	43
Total dihedral angle restraints	201	201	201
$^3J_{\text{HN}\alpha}$ scalar couplings	49	49	49
$^3J_{\text{HNC}'}^{\prime}$ scalar couplings	49	49	49
$^3J_{\text{HNC}\beta}$ scalar couplings	49	49	49
$^{13}\text{C}^\alpha$ chemical shifts	54	54	54
Structure statistics			
Average CYANA target function value (Å ²)	9.94	27.46	4.48
Violations			
Distance constraints (>0.5 Å)	2	6	0
Dihedral angle constraints (>5°)	1	1	1
Deviations from idealized geometry ^a			
Bond lengths (Å)	0	0	0
Bond angles (°)	0	0	0
Impropers (°)	0	0	0
Average pairwise r.m.s. deviation ^b (Å)			
Heavy atoms	0.86 ± 0.04	0.60 ± 0.06	0.87 ± 0.07
Backbone	0.47 ± 0.05	0.11 ± 0.04	0.47 ± 0.08
R.m.s. deviation to RDC-refined X-ray structure (Å)			
Heavy atoms	1.31	1.17	1.38
Backbone	0.72	0.57	0.95

^aStructure calculation in torsion-angle space with exactly maintained bond lengths, bond angles and impropers. ^bCalculated among 20 refined structures.

Figure 2 Target-function (TF) values of various ensemble-based structure calculations of GB3, highlighting the importance of the ensemble-based structure calculation (left) and the self-consistency of the data by cross-validations (right). The CYANA target function is the (weighted) sum of the squared violations of the conformational restraints. Left, target-function values versus number of simultaneously calculated states for all violations (blue) and for eNOEs only (red). Right, cross-validation tests highlighted by target functions. Shown in blue is the normalized target function obtained from a jackknife procedure that deletes 10% of all the experimental input data randomly ten times (see text). Target functions upon random alteration of the distances obtained from cross-peaks according to normal distributions with s.d. of 5% (yellow), 10% (orange) and 15% (red) or upon random alteration of all distances by 10% (pink) are shown. All these target-function values are substantially larger than those in the left panel, indicating that the original experimental data set is self-consistent.



included in the structure calculation. Most prominent is its decrease from one state, which corresponds to the conventional structure-calculation protocol (yet with eNOEs), to two and three states, after which a plateau is reached. This observation indicates that, in contrast to the single-structure, a three-state ensemble as represented in **Figure 1c** describes the experimental data well (backbone r.m.s. deviation of 0.46 Å and an all-heavy atom r.m.s. deviation of 0.82 Å). Higher-state ensembles also fulfill the experimental data, covering a conformational space very similar to that of the three-state ensemble (**Supplementary Figs. 2 and 3**). In the following, the three-state ensemble is used as a representative of the GB3 structure in solution because it is the smallest ensemble that fulfills the experimental data well. The input data represent a self-consistent set, and the restraints are well satisfied in the three-state ensemble (**Table 1**). To strengthen this finding, we arbitrarily changed all eNOE-derived distances by up to 15%, yielding considerable increases of the target functions (**Fig. 2**). This observation indicates that the eNOE-derived restraints have an accuracy much better than 15%, as demonstrated earlier^{16,17}. In addition, it shows that the experimental data set is self-consistent

and, at least in part, overdetermined, although the free parameter space was extensively enlarged with the introduction of the ensemble-based structure calculation. The need for multistate ensembles is further supported by a cross-validation test, which consists of the arbitrary deletion of 10% of all the eNOEs²⁸. The test shows that the violations of the nonincluded eNOE-derived distances summed over ten structure calculations (deleting every eNOE exactly once overall) decrease with the size of the ensemble, resulting in a drop of the target function by up to 40% when compared with that of the single-state structure (**Fig. 2**). These findings confirm the prediction, based on theoretical considerations, that very tight distance restraints (less than 25% error) are required in order to calculate a multistate structure²⁹. Finally, the close resemblance between local order parameters derived from the three-state ensemble and RDC-derived order parameters measured in a previous study²⁶ indicates that the three-state ensemble well represents the structural space covered by internal motions of GB3 (**Fig. 3** and unpublished data).

Following the arguments above, the three-state structural ensemble is a compact experiment-based representation of GB3 in solution. In contrast to the standard structure-determination protocol, it takes into account that the NOE is a time- and ensemble-averaged parameter yielding an ensemble representation of the structure covering the conformational space of GB3. Because of the bundling restraints present in the calculation, the multistate structure ensembles cover the minimal conformational space required to fulfill the experimental data.

A detailed inspection of the structural ensemble shows that the three structural states are distinct from each other. Individual-state sub-bundle representations were obtained by grouping the most similar structures from each three-state conformer (**Figs. 1 and 4**). The sub-bundle for each structural state is thereby a measure of the precision of the individual structural states, similar to the conventional bundle representation. Notably, the same bundle representation can be used for the entire β -sheet and some of the loops, indicating that

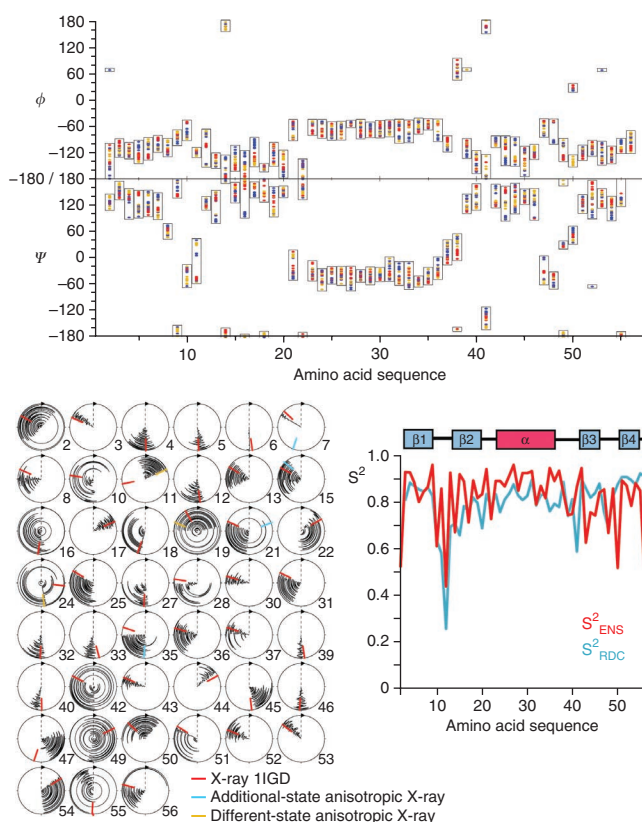


Figure 3 Structural space coverage of the ensemble-based structure of GB3.

Top, distribution of ϕ (top) and ψ (bottom) backbone angles versus the amino acid sequence. The angles are shown for the nine three-state conformers.

The most similar structures from each three-state conformer are grouped in yellow, red and blue. Anticorrelated behavior between ϕ (top) and ψ (bottom) is observed for many residues, such as residues two and four. Bottom right, backbone H^N -N order parameters versus amino acid sequence. Red values are computed from the three-state ensemble (S^2_{ENS}), and blue values are RDC-derived values (S^2_{RDC})²⁶. Bottom left, circle diagrams of the χ^1 angles obtained from a three-state ensemble represented by 20 conformers each.

The individual diagrams are labeled by the number of the corresponding residue. The corresponding angles from the X-ray structure 1IGD²⁵ are indicated in red. If the anisotropically evaluated X-ray structure 2IGD²⁵ shows a second angle in addition to the former, it is indicated in blue, and if it exhibits a different single state, in yellow.

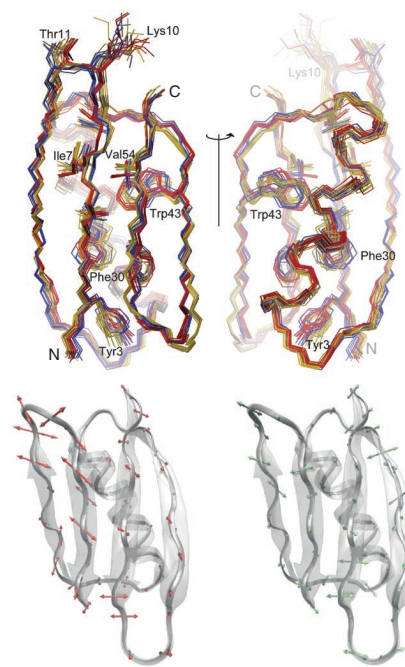
Figure 4 Structural representation of a three-state ensemble of GB3. Top, bundle representation of the three-state structure. The most similar structures from each three-state conformer are grouped in yellow, red and blue (as in **Fig. 3**). For each ensemble, nine conformers were selected. In addition to the backbone, the side chains of hydrophobic core residues and the two solvent-exposed residues Lys10 and Thr11 are also shown. The termini of the protein are also labeled. Bottom, first (left) and second (right) mode of principal component analysis. The arrows indicate directions and amplitudes (enlarged 5× for better visibility).

this entire structural segment undergoes conformational exchange between the three states in a concerted fashion. The central parallel β -sheet (strands $\beta 1$ and $\beta 4$) moves parallel to the entire β -sheet architecture (that is, vertically with respect to the polypeptide backbone) while the loops between $\beta 1$ and $\beta 2$, and $\beta 3$ and $\beta 4$, as well as between accompanied segments within the β -strands, counteract this motion in an anticorrelated manner (**Fig. 4** and **Supplementary Fig. 4**). A principal-component analysis (PCA) of the ensemble visualizes these findings further. In this analysis, the major part of the spatial sampling is covered by the first two PCA modes (**Supplementary Fig. 5**). This analysis describes concerted motion across the β -sheet, as indicated by the arrows in **Figure 4** that show the directions and amplitudes of the principal motions. In contrast, the α -helix appears to be decoupled from the conformational exchange of the β -sheet, as the bundle representation of the β -sheet does not enable us to distinguish several structural states of the α -helix (**Fig. 4**). However, another set of conformers selected to describe structural states of the α -helix indicates that the backbone of the α -helix shows also distinct structural states that interconvert between each other, but the correlation appears to be weaker than for the β -sheet and is localized to the residues that face the hydrophobic core (**Supplementary Fig. 4**). The rate of exchange between the conformational states in the β -sheet as well as in the α -helix is most likely on the sub-millisecond timescale because slower motion would result in line broadening or resonance doubling not observed in the spectra and because the three-state ensemble is consistent with the RDC-derived order parameters²⁶ sensitive to motion faster than the millisecond timescale (**Fig. 3**).

DISCUSSION

The eNOE-based ensemble presented here is in good agreement with previously obtained multiple-state ensembles^{2,5} calculated from relaxation order parameters, slow motion-sensitive RDCs and (in one case⁵) crystallographic B factors, although these ensembles appear to be optimally represented by 4–8 states rather than by the 3 states derived from the eNOE analysis. All three ensemble representations show a similar amplitude of structural variations described by r.m.s. differences between the states within the ensemble of around 0.5 Å. In all three ensembles, we observed crankshaft motions (anticorrelated ϕ_i and ψ_{i-1} angles) along the entire backbone and concerted structural variations in the β -sheet, with the largest correlated structural variations in the loops connecting strands $\beta 1$ and $\beta 2$, and the α -helix and $\beta 3$. The observations of concerted motions are further supported by other previous studies on GB3 or the similarly folded ubiquitin, using RDCs^{7,14} in combination with hydrogen-bond scalar couplings³ and cross-correlated relaxation (CCR) rates¹². For example, local anticorrelated motion between the ϕ and ψ backbone torsion angles within part of the β -sheet had also been observed¹⁴. Our three-state ensemble also shows such anticorrelated properties for these backbone angles (**Fig. 3**, top).

The observation of the distinct states of the backbone of GB3 can, in part, be extended to the side chains, as visualized, for example, for residues 3, 12 and 43, for which the side chains show distinct structural



states that correlate well with the distinct backbone states (**Fig. 4**). For most of the side chains in the hydrophobic core, such structurally distinct states can be seen, whereas some of the surface-faced side chains show arbitrary conformations, as exemplified by Lys11 (**Fig. 4**), indicative of either free motion or lack of sufficient experimental data. Similar findings can be visualized by the χ^1 angles that also describe the rotamer states of the side chains (**Fig. 3**). All but one of the side chains in the hydrophobic core have a single rotamer state that is in good agreement with the X-ray structure. Only residue 54, close to the C terminus, has two rotamer states for the χ^1 angle. Interestingly, the rotamers of residue 54 correlate well with the distinct backbone structural states of the last β -strand, indicating that the rotamers interchange in a concerted manner with the conformational exchange of the backbone. Outside the hydrophobic core, many residues have multiple χ^1 rotamer states. By correlating the χ^1 rotamer states with the distinct structural states of the backbone, it is possible to observe a coupling between them within the secondary structural elements, whereas most of the side chain rotamer states in the loops appear to be decoupled from their (local) backbone states.

In the following, the side chain rotamers are discussed in more detail. For residues 15, 21 and 35, the same two rotamer states were observed as in the crystal structure. Actually, the NMR ensemble includes all the rotamer states observed in the crystal structures, with the exception of residues 7 and 47, for which χ^1 deviates by roughly 40° (**Fig. 3**). Also, scalar and residual dipolar couplings as well as cross-correlated relaxation rates measured under liquid-state conditions are in very good agreement with the rotamer states of the structural ensemble including residues 7 and 47. For example, all but one of the rotamer states obtained from scalar couplings are in line with the structural ensemble. The only inconsistent rotamer state is χ^1 of residue 8, for which the ensemble has the same rotamer as the X-ray structure. Furthermore, the structural ensemble is in accord with measurements from a previous study³⁰, which determined the rotamer populations of χ^1 angles of valine, isoleucine and threonine by RDCs, $^3J_{C'CH}$ and $^3J_{NC\gamma}$ scalar couplings: for residues 3, 6, 7, 17, 18, 33, 39, 44 and 52, the single predicted rotamer states; for residues 21, 25, and 54, the two predicted rotamers; and for residue 42,

all three predicted rotamers are in line with the structural ensemble. Discrepancies are observed for residues 11, 49, 51 and 53. Overall, there is good agreement between the sampling in the ensemble and previously analyzed X-ray or NMR data. Some inconsistencies may have arisen from different sample conditions, such as crystalline or liquid state, or different buffer conditions.

In conclusion, by taking into account the motional dependence of the eNOE, we have established an ensemble-based NMR structure-determination protocol that results in a description of the conformational space of the protein of interest if a sufficient number of eNOEs are collected. The application to the protein GB3 shows distinct, albeit similar, structural states within the β -sheet and the accompanying loops that interchange, most likely, on the microsecond timescale, whereas the α -helix is decoupled from this motion. These findings indicate that the measurement of eNOEs opens an avenue toward a comprehensive spatial description of both the 3D structure and the motion of biomolecules, with the potential to uncover communication pathways among remote sites of a protein.

METHODS

Methods and any associated references are available in the online version of the paper.

Accession codes. The three-state ensemble NMR structure of GB3 has been deposited in the Protein Data Bank, accession code 2LUM.

Note: Supplementary information is available in the online version of the paper.

ACKNOWLEDGMENTS

We thank L. Wang (Laboratory of Physical Chemistry, Eidgenössische Technische Hochschule Zürich, Zürich) for the preparation of the GB3 NMR sample. P.G. gratefully acknowledges financial support from the Lichtenberg program of the Volkswagen Foundation.

AUTHOR CONTRIBUTIONS

B.V., P.G. and R.R. designed the study; B.V. conducted measurements; P.G. did the software programming; B.V., P.G., S.K. and R.R. analyzed the data.

COMPETING FINANCIAL INTERESTS

The authors declare no competing financial interests.

Published online at <http://www.nature.com/doi/10.1038/nsmb.2355>.

Reprints and permissions information is available online at <http://www.nature.com/reprints/index.html>.

1. Clore, G.M. & Schwieters, C.D. How much backbone motion in ubiquitin is required to account for dipolar coupling data measured in multiple alignment media as assessed by independent cross-validation? *J. Am. Chem. Soc.* **126**, 2923–2938 (2004).
2. Clore, G.M. & Schwieters, C.D. Amplitudes of protein backbone dynamics and correlated motions in a small α/β protein: correspondence of dipolar coupling and heteronuclear relaxation measurements. *Biochemistry* **43**, 10678–10691 (2004).
3. Lindorff-Larsen, K., Best, R.B., DePristo, M.A., Dobson, C.M. & Vendruscolo, M. Simultaneous determination of protein structure and dynamics. *Nature* **433**, 128–132 (2005).

4. Bouvignies, G. *et al.* Identification of slow correlated motions in proteins using residual dipolar and hydrogen-bond scalar couplings. *Proc. Natl. Acad. Sci. USA* **102**, 13885–13890 (2005).
5. Clore, G.M. & Schwieters, C.D. Concordance of residual dipolar couplings, backbone order parameters and crystallographic B-factors for a small α/β protein: a unified picture of high probability, fast atomic motions in proteins. *J. Mol. Biol.* **355**, 879–886 (2006).
6. Tang, C., Schwieters, C.D. & Clore, G.M. Open-to-closed transition in apo maltose-binding protein observed by paramagnetic NMR. *Nature* **449**, 1078–1082 (2007).
7. Markwick, P.R.L., Bouvignies, G. & Blackledge, M. Exploring multiple timescale motions in protein GB3 using accelerated molecular dynamics and NMR spectroscopy. *J. Am. Chem. Soc.* **129**, 4724–4730 (2007).
8. Lange, O.F. *et al.* Self-consistent residual dipolar coupling based model-free analysis for the robust determination of nanosecond to microsecond protein dynamics. *Science* **320**, 1471–1475 (2008).
9. Baldwin, A.J. & Kay, L.E. NMR spectroscopy brings invisible protein states into focus. *Nat. Chem. Biol.* **5**, 808–814 (2009).
10. Markwick, P.R.L. *et al.* Toward a unified representation of protein structural dynamics in solution. *J. Am. Chem. Soc.* **131**, 16968–16975 (2009).
11. Bui, J.M., Gsponer, J., Vendruscolo, M. & Dobson, C.M. Analysis of sub- μ s and supra- μ s motions in protein Gb1 using molecular dynamics simulations. *Biophys. J.* **97**, 2513–2520 (2009).
12. Vögeli, B. & Yao, L. Correlated dynamics between HN and HC bonds observed by NMR cross relaxation. *J. Am. Chem. Soc.* **131**, 3668–3678 (2009).
13. Shaw, D.E. *et al.* Atomic-level characterization of the structural dynamics of proteins. *Science* **330**, 341–346 (2010).
14. Fenwick, R.B. *et al.* Weak long-range correlated motions in a surface patch of ubiquitin involved in molecular recognition. *J. Am. Chem. Soc.* **133**, 10336–10339 (2011).
15. Wüthrich, K. *NMR of Proteins and Nucleic Acids* (Wiley, 1986).
16. Vögeli, B. *et al.* Exact distances and internal dynamics of perdeuterated ubiquitin form NOE buildups. *J. Am. Chem. Soc.* **131**, 17215–17225 (2009).
17. Vögeli, B., Friedmann, M., Leitz, D., Sobol, A. & Riek, R. Quantitative determination of NOE rates in perdeuterated and protonated proteins: practical and theoretical aspects. *J. Magn. Reson.* **204**, 290–302 (2010).
18. Olejniczak, E.T., Dobson, C.M., Karplus, M. & Levy, R.M. Motional averaging of proton nuclear Overhauser effects in proteins. Predictions from a molecular dynamics simulation of lysozyme. *J. Am. Chem. Soc.* **106**, 1923–1930 (1984).
19. Keepers, J.W. & James, T.L. A theoretical study of distance determinations from NMR. Two-dimensional nuclear Overhauser effect spectra. *J. Magn. Reson.* **57**, 404–426 (1984).
20. Brüschweiler, R. *et al.* Influence of rapid intramolecular motion on NMR cross-relaxation rates. A molecular dynamics study of antamanide in solution. *J. Am. Chem. Soc.* **114**, 2289–2302 (1992).
21. Leitz, D., Vögeli, B., Greenwald, J. & Riek, R. Temperature dependence of $^1\text{H}^{\text{N}}\text{--}^1\text{H}^{\text{N}}$ distances in ubiquitin as studied by exact measurements of NOEs. *J. Phys. Chem. B* **115**, 7648–7660 (2011).
22. Koning, T.M.G., Boelens, R. & Kaptein, R. Calculation of the nuclear Overhauser effect and the determination of proton-proton distances in the presence of internal motions. *J. Magn. Reson.* **90**, 111–123 (1990).
23. Güntert, P., Mumenthaler, C. & Wüthrich, K. Torsion angle dynamics for NMR structure calculation with the new program DYANA. *J. Mol. Biol.* **273**, 283–298 (1997).
24. Güntert, P. Automated structure determination from NMR spectra. *Eur. Biophys. J.* **38**, 129–143 (2009).
25. Derrick, J.P. & Wigley, D.B. The third IgG-binding domain from streptococcal protein G: an analysis by X-ray crystallography of the structure alone and in a complex with Fab. *J. Mol. Biol.* **243**, 906–918 (1994).
26. Yao, L., Vögeli, B., Torchia, D.A. & Bax, A. Simultaneous NMR study of protein structure and dynamics using conservative mutagenesis. *J. Phys. Chem. B* **112**, 6045–6056 (2008).
27. Brüschweiler, R., Blackledge, M. & Ernst, R.R. Multi-conformational peptide dynamics derived from NMR data: a new search algorithm and its application to antamanide. *J. Biomol. NMR* **1**, 3–11 (1991).
28. Brünger, A.T., Clore, G.M., Gronenborn, A.M., Saffrich, R. & Nilges, M. Assessing the quality of solution nuclear magnetic resonance structures by complete cross-validation. *Science* **261**, 328–331 (1993).
29. Bonvin, A.M.J.J. & Brünger, A.T. Conformational variability of solution nuclear magnetic resonance structures. *J. Mol. Biol.* **250**, 80–93 (1995).
30. Chou, J.J., Case, D.A. & Bax, A. Insights into the mobility of methyl-bearing side chains in proteins from $^3\text{J}_{\text{CC}}$ and $^3\text{J}_{\text{CN}}$ couplings. *J. Am. Chem. Soc.* **125**, 8959–8966 (2003).

ONLINE METHODS

NMR experiments and analysis. GB3 was expressed and purified as described previously³¹. The ¹³C,¹⁵N-labeled NMR sample contained 350 µl of 4 mM protein solution in 97% H₂O, 3% D₂O, 50 mM potassium phosphate buffer, pH 6.5, and 0.5 mg/ml sodium azide.

All experiments were performed on a Bruker 700-MHz spectrometer equipped with a triple-resonance cryoprobe at 298 K. A series of 3D [¹⁵N,¹³C]-resolved [¹H,¹H]-NOESY spectra was recorded for the measurement of NOE buildups. A spectrum with $\tau_{\text{mix}} = 100$ ms was used for adapting the resonance assignment. Diagonal-peak decay and cross-peak buildup were followed with a series of 1-d experiments with $\tau_{\text{mix}} = 20, 30, 40, 50$ and 60 ms. All spectra were processed and analyzed by using the software packages NMRPipe³² and NMRDraw³³. The cross-relaxation rates were extracted using the protocol established previously with in house-written software and the DOMINO program¹⁹.

Structure determination. Structure calculations were done with the program CYANA on the basis of the experimental restraints listed in **Supplementary Tables 1 and 2**. Calculations were started from 100 conformers with random torsion-angle values, simulated annealing with 50,000 torsion-angle dynamics steps was applied and the 20 conformers with the lowest final target-function values were analyzed. For the ensemble-averaged calculations, 2–9 structural states of the entire protein were calculated simultaneously, excluding steric repulsion between atoms of different states and applying the eNOE distance restraints to the $1/r^6$ averages of the corresponding distances in the individual states. Similarly, the ³J-coupling restraints and the RDC restraints were applied to the arithmetic means of the corresponding quantities in the individual states. Bundling restraints were applied in order to keep the individual structural states together in space, as far as permitted by the experimental restraints. To this end, weak upper distance bounds of 1.2 Å were imposed on all distances between the same nitrogen and carbon atoms in different states. The weight of these bundling restraints was 100 times lower than for NOE upper distance bounds, except for the backbone atoms N, C^α, C' and C^β, for which a weight ten times lower than for NOEs was used. The single- (or three-) state ensemble has 92.0% (81.6%), 7.9% (16.9%),

0.0% (1.1%) and 0.1% (0.4%), respectively, in the most favored, additionally allowed, generously allowed and disallowed regions of the Ramachandran plot. The corresponding values for the conventional calculation are 88.9%, 9.0%, 2.1% and 0.0%. The three-state ensemble NMR structure of GB3 has been deposited in the Protein Data Bank, accession code 2LUM.

PCA of the eNOE-derived structure bundle. To elucidate correlated backbone motions, the C^α atom positions in the eNOE-derived three-state ensemble of GB3 were analyzed by PCA. The conformers in the ensemble were superimposed for minimal r.m.s. deviation between the C^α atoms and the corresponding mean structure, and the resulting coordinates were subjected to PCA³⁴ using the Python package ProDy³⁵ for the calculation of the superposition to the mean, the covariance matrix and the singular value decomposition. The covariance matrix was diagonalized to determine the principal modes of structural variations observed in the ensemble. The principal modes were rank ordered by the size of the corresponding eigenvalues (**Supplementary Fig. 5**). PCA mode 1 refers to the direction of maximal variance, followed by PCA mode 2, etc. To illustrate the correlated motions of the backbone, the eigenvectors of the first and second principal modes were depicted using the molecular graphics package VMD³⁶ (**Fig. 4**, arrows attached to the mean C^α positions).

31. Ulmer, T.S., Ramirez, B.E., Delaglio, F. & Bax, A. Evaluation of backbone proton positions and dynamics in a small protein by liquid crystal NMR spectroscopy. *J. Am. Chem. Soc.* **125**, 9179–9191 (2003).
32. Delaglio, F. *et al.* NMRPipe: a multidimensional spectral processing system based on UNIX pipes. *J. Biomol. NMR* **6**, 277–293 (1995).
33. Johnson, B.A. & Blevins, R.A. A computer program for the visualization and analysis of NMR data. *J. Biomol. NMR* **4**, 603–614 (1994).
34. Bakan, A. & Bahar, I. The intrinsic dynamics of enzymes plays a dominant role in determining the structural changes induced upon inhibitor binding. *Proc. Natl. Acad. Sci. USA* **106**, 14349–14354 (2009).
35. Bakan, A., Meireles, L.M. & Bahar, I. ProDy: protein dynamics inferred from theory and experiments. *Bioinformatics* **27**, 1575–1577 (2011).
36. Humphrey, W., Dalke, A. & Schulten, K. VMD: visual molecular dynamics. *J. Mol. Graph.* **14**, 33–38 (1996).